Heliyon 7 (2021) e07269

Contents lists available at ScienceDirect

Heliyon

journal homepage: www.cell.com/heliyon

Research article

Effect of annealing temperature on structural, optical, and photocatalytic properties of titanium dioxide nanoparticles

Dorah Kawira Muthee [a,b,*], Birhanu Francis Dejene [c]

[a] Department of Physics, University of the Free State (QwaQwa Campus), Private Bag, X13, Phuthaditjhaba, 9866, South Africa
[b] Machakos University, P.O box 136-90100, Machakos, Kenya
[c] Physics Department, Walter Sisulu University (Mthatha Campus), Private Bag X1, South Africa

ARTICLE INFO

Keywords:
Ti^{3+}
Photocatalysis
Crystallinity
Mixed-phase
Sol-gel method

ABSTRACT

Titanium dioxide (TiO_2) nanoparticles (NPs) were produced by simple sol-gel technique and annealed for 2 h in air. The impact of annealing temperature on the physical, morphological, photocatalytic, and optical properties was studied. X-ray diffraction (XRD) measurements proved that a gradual phase change from anatase to rutile occurred with increased annealing temperature. The crystal structures of the NPs were found to change at different temperatures; anatase phase at 450 °C, mixed-phase (anatase/Rutile) at 550–650 °C, and rutile phase at 750 °C. The rise in the annealing temperature improved the crystallinity of the NPs. The crystal and grain size of the NPs increased with the annealing temperature hence reducing the specific surface area due to the condensed boundaries between subunits of the NPs. As per the Kubelka-Munk equation, the bandgap reduced as the temperature elevated. The photocatalytic activity of the NPs was higher in the anatase/rutile mixed-phase than in the single anatase and rutile phase. Experimental results indicated that annealing temperature could effectively change the properties of the TiO_2 NPs.

1. Introduction

Titanium dioxide (TiO_2) is considered an appealing nanomaterial due to its versatility. TiO_2 is polymorphic and exists in three major crystalline structures in nature; anatase with a refractive index of 2.49, brookite with a refractive index of 2.58, and rutile with a refractive index of 2.61 [1,2]. It also exists in mixed phases of rutile-anatase, anatase-brookite, and anatase-brookite-rutile phase [3]. Suggestions show that nanomaterial application depends highly on the crystal phase, morphology, and crystal size [4]. Rutile and anatase phases have been widely reported as photocatalysts. We also observed the enhanced high photoactivity of the mixed anatase-rutile phase in our previous work [5]. In a mixed-phase, the flow of electrons from the anatase to a lower-energy rutile trapping site could limit charge carrier recombination and efficiently establish catalytic "hot spots." Just a few brookite reports have been made for the past years due to low photocatalytic activity [6]. Under UV/visible light illumination, TiO_2 can catalytically degrade pollutants in water such as dyes, benzine, and contaminants in complex mixtures found in domestic and industrial effluents [7]. To prepare TiO_2 with the desired properties, various techniques such as sol-gel, solvothermal, hydrothermal, and hydrolytic precipitation have been used [8, 9]. Among other techniques, sol-gel is the most appropriate because it can make nanomaterials with required surface properties and control reaction at low temperatures [10]. The rutile phase is thermodynamically stable, unlike the metastable anatase and brookite phases. The metastable phases are found to transform to the rutile phase at different conditions, such as high annealing temperatures [11]. A.K.M. Muaz et al. annealed thin films at 300 °C, 500 °C for 1 h and observed a slight transformation from anatase to rutile at 500 °C. A.S Bakri et al. [12] suggested that anatase/rutile phase transformation occurred at temperatures greater than 900 °C after annealing thin films for 1 h. Nanopowders also annealed at 600 °C, 700 °C, and 800 °C for an hour by S. Mathur et al. showed phase transformation at which the rutile phase dominated at 800 °C. According to M.K. Singh et al. [13], there was a total anatase to rutile phase transformation at 800 °C. It is clear that the influence of the annealing temperature on the TiO_2 properties have not been exhaustedly studied. The intention for this study was to examine the effect of annealing for 2 h at (450 °C, 550 °C, 650 °C, 750 °C) on the structural, crystal size, morphological, optical, and photocatalytic properties of the synthesized TiO_2 NPs by sol-gel technique. The photocatalytic activity was tested by degrading methylene blue using artificial

* Corresponding author.
E-mail address: kawirahdorah@gmail.com (D.K. Muthee).

https://doi.org/10.1016/j.heliyon.2021.e07269
Received 8 May 2020; Received in revised form 4 January 2021; Accepted 7 June 2021

UV light. Hence being able to suggest from our study the best photocatalyst for water purification.

2. Methods

2.1. Chemicals

All of the reagents used were of analytical grade purity and were used precisely as supplied by the manufacturer. Tetra isopropyl orthotitanate ($C_{12}H_{28}O_4Ti$) purity >98% from Aldrich was used as titanium precursor, ethanol absolute (C_2H_6O), purity (>99.9%) as a solvent medium, and ethanolamine as a catalyst.

2.2. Synthesis procedure

TiO_2 NPs were prepared by the sol-gel method with 11 mL of tetra isopropyl orthotitanate (TIP) and 62.8 mL of ethanol. After making a solution and vigorously stirring for 2 h (h), 10 mL of (ethanol + deionized (DI) water) was added dropwise under agitation. After that, the sol was aged for 24 h, and the formed gel dried at 130 °C for 2 h. Finally, the samples were annealed at 450 °C, 550 °C, 650 °C, and 750 °C for 2 h to obtain the desired NPs. To allow the reusability of the TiO_2 photocatalyst, the powder was converted into pellets.

2.3. Photocatalytic test

The samples obtained at different thermal treatments were photocatalytically tested using methylene blue dye under UV light radiation. To achieve the adsorption-desorption equilibrium, 2 g/L TiO_2 pellets were suspended in methylene blue solution and continuously stirred for 0.5 h. The UV light was used to irradiate the samples in a normal direction by placing it above the samples. The degradation of MB was carried out for 2 h, with a close track by taking a 5 mL sample every 0.25 h using the Shimadzu-1700 UV-vis spectrophotometer. MB degradation was estimated by adsorption peak at 664 nm [14].

2.4. Characterization of the samples

Philips Bruker D8 advance X-ray diffractometer, Cu Kα X-ray (λ = 1.5406 Å) was used at 40 kV, 30 mA, at a scanning range of 20–60° to obtain the crystal structure and the phase of the synthesized TiO_2 NPs. Debye-Scherer's equation was used to calculate crystal sizes [15]. Identification of the crystalline phase was made based on the joint committee powder diffraction standard (JCPDS). Morphology and the composition of the NPs were investigated using Tescan Vega 3 Scanning Electron Microscopy (SEM) and Oxford X-Max^N Energy Dispersive Spectroscopy (EDS), respectively. The diffuse reflectance was done using a lambda 950 spectrometer for the bandgap estimation. The PL spectra of the synthesized TiO_2 powders were recorded at room temperature using 320 nm excitation light on a Fluorescence Spectrophotometer (F-7000).

3. Results and discussion

3.1. XRD analysis

The X-ray diffraction (XRD) patterns of all the samples, annealed at different temperatures, were depicted in Figure 1. The peaks were referenced according to #861157 (anatase) and #860147 (rutile) phase. After annealing at 450 °C for 2 h, anatase peaks emerged with a small brookite peak observed. The optimal peak intensities of the anatase phase were observed at 550 °C thermal annealing, after which 650 °C temperature caused a drastic decrease in intensities with an appearance of the peaks from the rutile phase. As the temperature increased, mixed anatase-rutile peaks were observed, with a small peak from brookite detected between 550 °C and 650 °C. Thus, the total transformations to the rutile phase occurred at 650 °C. During this change from (anatase to

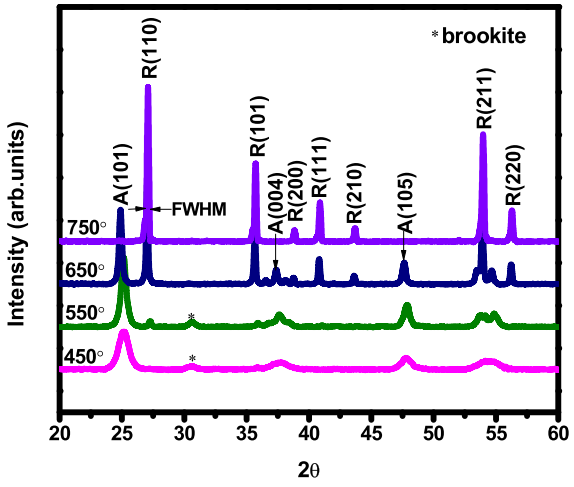

Figure 1. XRD patterns for TiO_2 NPs calcined at various temperatures.

rutile), there was a phenomenon of polymorphs reconstructing due to the assembling of the atoms and the wide-range reorganization of the bonds of the particles [10]. Therefore, the phase transformation due to varied annealing temperatures was as shown in Eq. (1).

$$\text{Amorphous} \rightarrow \text{Anatase} \rightarrow \text{anatase/rutile} \rightarrow \text{Rutile} \quad (1)$$

The mole ratios of the anatase and rutile phases were calculated based on the Spurr and Myers Eqs. (2) and (3) using the most intense peak of each phase [5].

$$W_R = \frac{1}{1 + 0.8(I_A/I_R)} \quad (2)$$

$$W_A = 1 - W_R \quad (3)$$

W_R and I_R represent the mole fraction and intensity of the rutile phase while W_A and I_A are the mole fraction and intensity of the anatase phase. The phase content of anatase (101) and rutile (110) was obtained using Eqs. (4) and (5) [16].

$$Anatase\% = \frac{100 \times I_A}{I_A + 1.265 \times I_R} \quad (4)$$

$$100 - A\% = Rutile\% \quad (5)$$

I_A and I_R represent the intensity of the anatase (101) and rutile (110) phases. When a comparison was made between the two methods, a slight difference was found, associated with each technique's nature. However, the result obtained portrayed a similar trend and was very near, as shown in figure 2(a) and (b) [17].

The effect of thermal treatment was depicted in Figure 2 based on the mole fraction and phase content of anatase and rutile phase. It is observed that both phases are reciprocal to each other. Therefore, we can suggest that anatase content decreases with an increase in annealing temperature while rutile content increases. The Debye-Scherrer [15] Eq. (6) was used to estimate the average crystal size (D) of the TiO_2 nanoparticles.

$$D = \frac{0.9\lambda}{\beta cos\theta} \quad (6)$$

β represents the full width at half maximum, λ is the X-ray wavelength (1.506 Å), while θ is the diffraction angle.

According to Figure 3(a), the crystallite sizes are inversely proportional to the FWHM. However, Figure 3(b) shows that the peak intensities of the TiO_2 nanoparticles increase with the rise in annealing temperature, which was an indication of improved crystal quality [18,

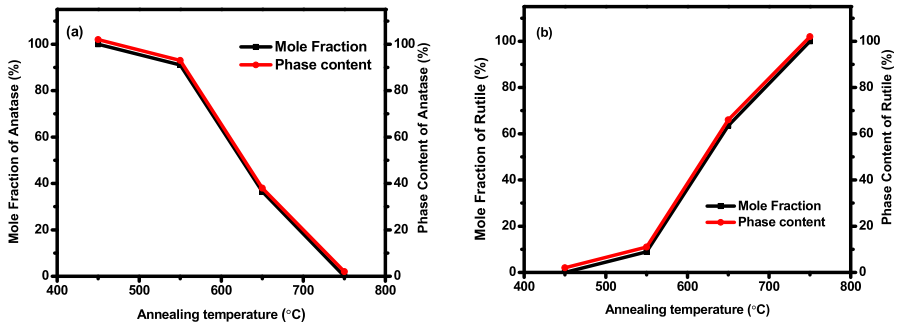

Figure 2. Mole content/phase content of TiO_2 (a) anatase phase and (b) rutile phase at various annealing temperatures.

19]. A relation was identified between peak intensity, crystallite size, and the FWHM as given by $Crystal\ size \propto \frac{Peakintensity}{FWHM}$. The crystal growth was attributed to thermally promoted crystallite growth. This parameter (annealing temperature) improves the crystalline structure by rearranging the atoms increasing the particle size of the TiO_2 nanoparticles [20]. There was a slow growth rate of particle sizes at lower temperatures, whose growth speed increased at higher temperatures. The rate at which crystal growth took place can be estimated using Eq. (7) [21].

$$V = D.\nu\left[\exp(-Q/KT)\right]\left[1-\exp\left(\frac{\Delta fv}{KT}\right)\right] \tag{7}$$

where $D$is the crystal size $\upsilon$is the frequency of the atoms' mutation, $Q$is the atoms' activation energy that attaches itself to the growing phase after leaving its network, and Δfv is the molar free energy difference between the two phases. Eq. (7) can be modified in cases of non-crystalline materials to form Eq. (8).

$$V = D.\nu\left[\exp\left(-\frac{Q}{KT}\right)\right] \tag{8}$$

This is because Δfv is much greater than KT. At low annealing temperatures, the activation energy is too high hence reducing the growth rate. While at a high annealing temperature, the initiation energy is too low, increasing the growth rate. According to the crystal size obtained using the Debye-Scherer equation, the difference in the anatase and rutile crystal size revealed that the nucleation and growth of the rutile phase would be initiated between 550 °C and 750 °C [21]. Nevertheless, the rate of phase transformation from anatase to rutile is very low for nanosized crystals due to the high surface area energy [22]. It has been mainly reported that the initiation and end temperature that causes the transformation of phases is between 600 °C and 900 °C [8]. It can be assumed that rutile growth starts right after nucleation. At 750 °C there is a complete elimination of the anatase phase and what is left is only the larger rutile crystals [23]. The specific surface area (SSA) was calculated by considering the total area covered by the crystals in unit mass. This was done with the help of Eq. (9), according to [16].

$$SSA = \frac{6\times10^3}{\rho D_p} \tag{9}$$

The density (4.23 g cm^{-3}) of TiO_2 nanoparticles was denoted by ρ, while D_p denotes the crystals size obtained by the Debye-Scherrer equation. The crystallographic defects or irregularities formed during crystal formation give rise to dislocations. Therefore, dislocation density (ρ) is the length of the dislocation lines per unit volume of the material crystal calculated using Eq. (10) [16].

$$\rho = \frac{1}{D_p^2} \tag{10}$$

Crystalline per unit surface area (N) is also an essential structural parameter determined using Eq. (11) [16].

$$N = \frac{d}{D_p^3} \tag{11}$$

where $D$is the size of the NPs while d is the inter-planar spacing between atoms.

SSA for anatase phase changes from 356.39 $m^2\ g^{-1}$ to 51.91 $m^2\ g^{-1}$ and that of the rutile phase changes from 34.45 $m^2\ g^{-1}$ to 48.84 $m^2\ g^{-1}$. According to Figure 4(a) and (b), a decrease in SSA for both the anatase and rutile phase was observed when the annealing temperature was raised. An inverse correlation between crystal size and SSA is observed [24]. The SSA and the photogenerated electron-hole pair recombination is crystal size-dependent. By increasing the specific surface area, the reactants' adsorption over the photocatalyst and light absorption will increase [25].

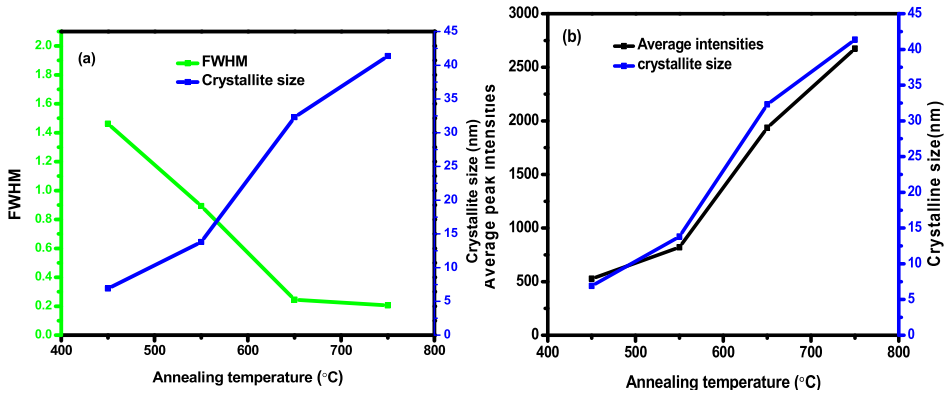

Figure 3. Impact of annealing temperature on TiO_2 average (a) crystallite size and FWHM, (b) crystallite size and peak intensities.

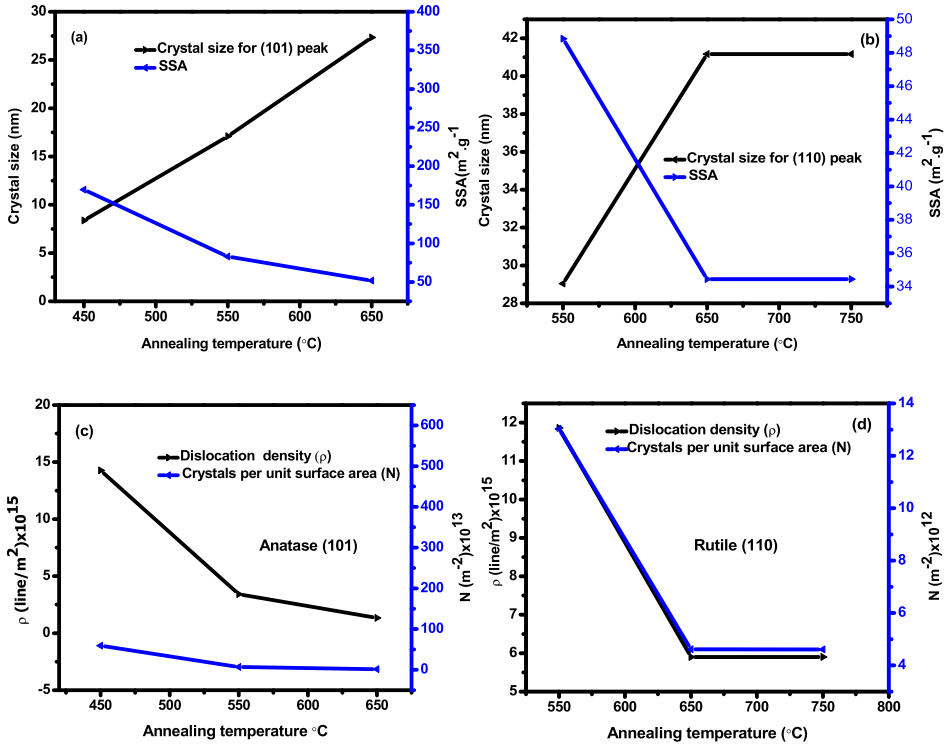

Figure 4. Effect of annealing temperature on (a) and (b) crystal size and SSA, (c) and (d) crystals per unit surface area and dislocation density of TiO_2 anatase (101) and rutile (110) peaks.

Figures 4(c) and (d) show that by increasing the annealing temperature on the TiO_2 nanoparticles, dislocation density and crystallite per unit surface area decreased. This is an indication that the temperature rise influences a decrease in dislocation density in crystallite sizes. Annealing temperature can produce a subtle effect on the morphology of TiO_2 NPs.

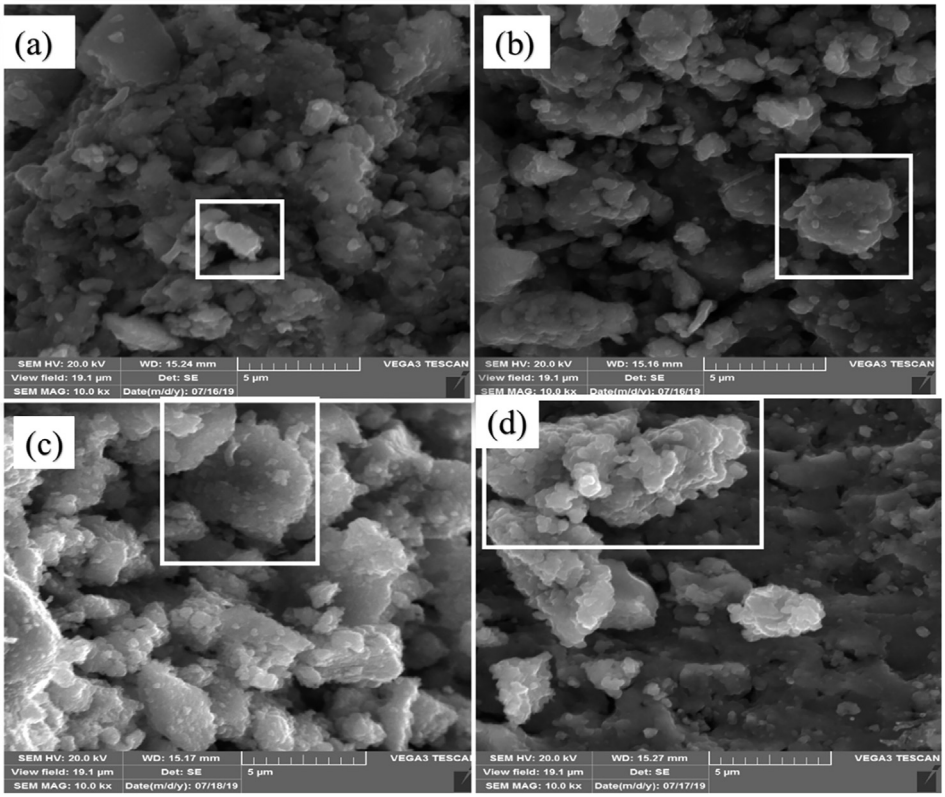

Figure 5. SEM images of samples at (a) 450 °C, (b) 550 °C, (b) 650 °C, and (c) 750 °C annealing temperatures.

3.2. SEM analysis

According to Figure 5, the annealing temperature encourages grain size growth [26]. However, aggregation was evident in the samples and was more pronounced at the annealing temperature of 750 °C. The particle sizes that can be recognized on a nanometer-scale are the primary particles, and their agglomerations are termed secondary particles. The agglomerations might be due to the overlapping of the small and medium particles, which have been caused by various kinds of forces such as weak surface force (soft agglomerates), strong chemical bonds (hard agglomerates), and lack of water on the surface structures [16, 27]. The annealing temperature interferes with the crystal structure and the material's morphology, which affects the specific surface area. These SEM results agree with the results obtained from XRD analysis that the crystal sizes increase with raised annealing temperature.

3.3. EDS analysis

Figure 6 displays the elemental composition of the synthesized material with some carbon traces [19]. The presence of a carbon trace in the results may indicate contamination from carbon tape during the measurements. The sample annealed at 450 °C has an atomic % of 33.88 (Ti) and 66.12 (O) near Ti and O's theoretical yields, 33.33% and 66.67%, respectively. The EDS results confirm the formation of TiO_2 as in XRD and SEM [21]. Figure 7 displays the effect of annealing temperature on the Ti and O elements of TiO_2 obtained from the EDS measurements. At about 675 °C, the ratios are stoichiometric, which agrees with XRD findings for the transformation of anatase to rutile phase, which begins at 650 °C. The findings show that the ideal temperature to achieve the TiO_2 anatase phase was between 450 °C and 650 °C. It is observed from Table 1 that with an increase in annealing temperature, the titanium proportion increase from 23.52 to 88.53 at% while the oxygen proportion decreased from 76.48 to 11.47 at%. This revealed that oxygen vacancies were driven and moved to Ti^{4+} ions, creating additional Ti^{3+} species, increasing oxygen vacancies' concentration as the calcination temperature raised [28]. Because Ti^{3+} ions are usually produced by the transfer of electrons trapped in oxygen vacancies to neighboring Ti

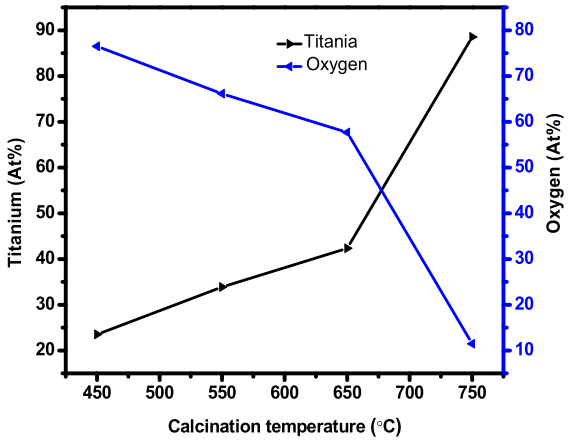

Figure 7. Elements percentage of Ti and O of samples annealed at 450 °C, 550 °C, 650 °C, and 750 °C temperatures.

atoms, Ti^{3+} ions in TiO_2 also indicate the presence of oxygen vacancies in the material. Using standard Kroger-Vink notation [29], the equilibrium in Eq. (12) can describe the formation of the oxygen vacancies at increased temperatures:

$$O_o \leftrightarrow^{TiO_2} V_o + \frac{1}{2}O_2(g) + 2e \tag{12}$$

The equilibrium constant of the reaction can be expressed as in the equation below [28].

$$k = [V_2]\, n^2 P(O_2)^{1/2} \tag{13}$$

According to the transformation of Eq. (13) oxygen vacancy concentration can be stated as a function of, $P(O_2)$ [28] in Eq. (14).

$$[V_2] = Kn^{-2} P(O_2)^{\left(-\frac{1}{2}\right)} \tag{14}$$

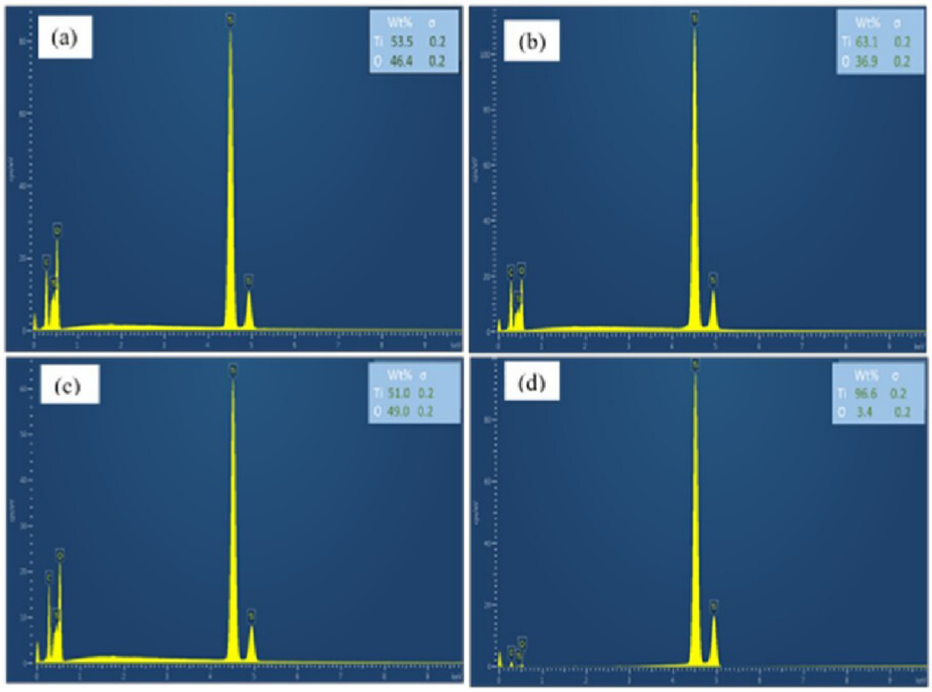

Figure 6. EDS Spectra for samples annealed (a) 450 °C, (b) 550 °C, (c) 650 °C, and (d)750 °C annealing temperatures.

Table 1. Data for EDS analysis.

Sample ℃	Atoms	Weight (%)	Atomic (%)
450	Ti	53.5	23.52
	O	46.4	76.48
550	Ti	63.1	33.88
	O	36.9	66.12
650	Ti	51.0	42.34
	O	49.0	57.66
750	Ti	96.6	88.53
	O	3.40	11.47

where O_0 denotes the lattice oxygen, V_o vacancies, $[V_o]$ represents the oxygen vacancy concentration; $P(O_2)$ designates the pressure of the oxygen vacancy. A decrease in the pressure of O_2 as seen in Eq. (14), oxygen vacancy concentration increases, such that in conditions with exhausted oxygen, annealing temperature would enable the creation of oxygen vacancies. Due to Eq. (12) reversible condition when TiO_2 is exposed in the air at ambient temperature, we consider doping in our subsequent work with ions' acceptor-type to stabilize the oxygen vacancies.

3.4. Optical analysis

Figure 8(a) depicts diffuse reflectance spectra with a wavelength between 600 and 200 nm of all samples synthesized by the sol-gel method. There was an elevation in the percentage reflectance of the nanoparticles from 36.75 % at an annealing temperature of 750 °C to 58.87 % (highest) at 550 °C. The Kubelka-Munk formula F(R) in Eq. (15) was used to estimate the bandgap of the TiO_2 [30].

$$F(R) = \frac{(1-R)^2}{2R} \tag{15}$$

A graph of $(F(R)\ hv)^2$ vs hv was plots to obtain the bandgap of the synthesized NPs as shown in Figure 8(b), where hv represents photon energy. Extrapolating a line from the curve's highest slope to the x-axis yields the bandgap [31]. As the annealing temperature rised, the crystal size increased resulting in a decrease in the bandgap hence approving the XRD analysis. A large crystal size gives a smaller bandgap, and vice versa is true [19]. The estimated bandgap ranges from 3.05 to 3.21 eV.

Higher annealing temperatures yield larger crystal sizes that influence the nanomaterial's specific surface area, affecting the light scattering. However, crystal sizes and the nature of phases play a serious role in adjusting the bandgap. Reduced interatomic spacing and structural changes have been responsible for lowering bandgap energies as annealing temperature rises. The thermal strains and the quantum size impact experienced in the annealing system greatly influence the bandgap energies. The reduced bandgap energies at raised annealing temperatures confirm the increase in grains as observed in SEM images.

3.5. Photoluminescence analysis (PL)

The generated electron-hole pair in the TiO_2 nanoparticles get trapped in the defect sites as they move to the surface for a redox reaction, enhancing their lifetime. It has been reported that the shallow traps formed by the defect states in the TiO_2 are advantageous in the electron-hole separation by promoting diffusion to the surface, while the deep traps enhance the recombination of the carriers [32]. Figure 9(a) shows the intense PL emission around 391 nm from all the synthesized samples excited at a wavelength of 340 nm in ambient temperature. The peak intensities were observed to decrease at raised annealing temperature, attributed to the structural transformation of TiO_2 because of the rise in order (in a medium-order range) and the tensile stress experienced by the nanomaterials [33]. Deconvolution was done based on pseudoVoigit fit for the sample at 750 °C annealing temperature yielding 380 nm, 391 nm, and 347 nm emission peaks as shown in Figure 9(b). The peak at 380 nm was credited to direct electron-hole recombination from the valence band to the conduction band of the nanomaterial. The other two peaks were ascribed to the defect states attributed to the transfer of charges from the Ti^{3+} to the oxygen anion in the TiO_6 associated with the oxygen vacancies. It is somewhat understandable considering that high temperatures give rise to oxygen vacancies that facilitate the formation of the Ti^{3+} when the anatase phase transforms fully to the rutile phase [34]. Charge carrier lifetime is one of the critical factors that highly influence the photo-activity of the TiO_2 nanoparticles depending greatly on the defect levels. The charge recombination phenomena are better studied

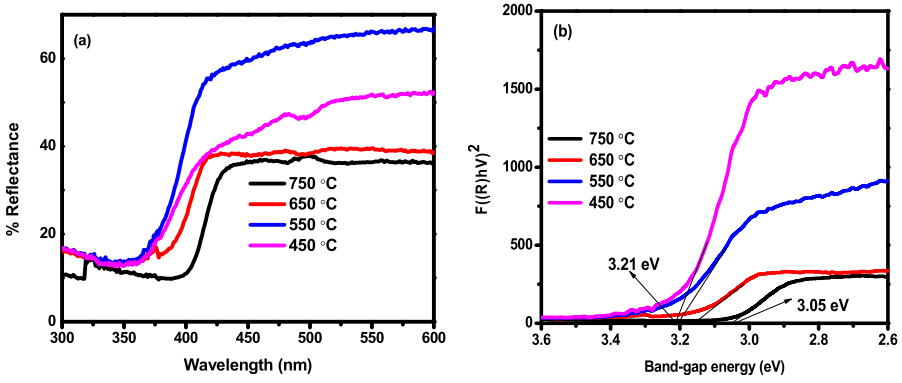

Figure 8. (a) Diffuse reflectance spectra of TiO_2 nanoparticles at different annealing temperatures, (b) Bandgap estimation using $(F(R)hv)^{)2}$ against hv in relation to the Kubelka-Munk equation.

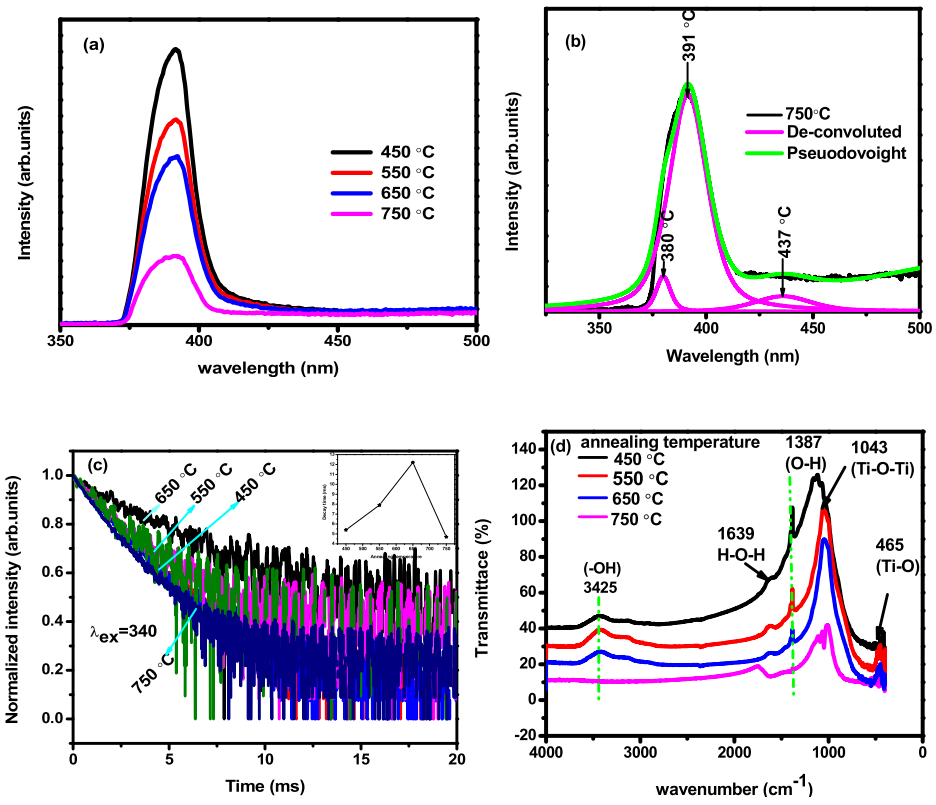

Figure 9. (a) PL Emission spectra for TiO_2 samples annealing at different temperatures (b) a deconvoluted graph of the sample annealed at 750 °C temperature, (c) PL decay curves for TiO_2 samples annealed at different temperatures, (d) FTIR spectra on the effect of annealing temperature on the functional groups of TiO_2 nanoparticles.

using time-resolved photoluminescence (TRPL). The decay curves of all samples were fitted using the single exponential function in Eq. (16) [35].

$$I = I_0 t\, exp\left\{-\frac{t}{\tau}\right\} \tag{16}$$

where I and I_0 are the intensities at time t and zero milliseconds, respectively, and τ is the lifetime. The Eq. (16) suggests carrier trapping sites of varying energy levels, resulting in a carrier transport rate distribution. Although the morphologies and the crystal sizes of the TiO_2 NPs were altered during the annealing process, the observed change of the visible lifetime on the millisecond time scale could not be attributed to particle size changes or particle morphology. According to Figure 9(c), the decay time increased with the annealing temperature and decreased at 750, ℃ as summarized in top-right insets. Low annealing temperature reduces the non-radiative recombination of the carriers due to the defects introduced during the synthesis hence increasing the decay time. The observed decrease at 750 °C was caused by the aggregations on the particles and the rutile formation at raised annealing [35], leading to an increased recombination process.

3.7. FTIR analysis

FTIR technique was used to analyze chemical functional groups and chemicals present in the samples. Figure 9 (d) depicts the FTIR spectra of TiO_2 NPs obtained at the range of 4000–400 cm^{-1}. The absorption band among wavenumber variety 3450–3400 cm^{-1} is due to the stretched vibration of surface hydroxyl groups –OH [36]. The peaks revealed that the sample dried at 450 °C contains some absorbed water molecules, which disappear with an increased annealing temperature. The absorption band observed at 1639 cm^{-1} and 1387 cm^{-1} are characteristic of O–H of water's bending vibration mode associated with surface adsorbed water [37]. NPs with a large surface area can absorb a large amount of water at specific active sites on the surface, resulting in the formation of NPs Ti $^{4+}$ $^{-}OH_2$ on the surface. The adsorbed water molecules produce a significant amount of heat, which aids in transforming TiO_2 from anatase to rutile. As the annealing temperature increases, the breakdown of the H–O–H bonds attached to Ti^{4+} occur thus the negatively charged O_{2-} participates in the formation of new Ti^{4+} bonds. Therefore, water molecules bound to Ti^{4+} at the interface and on the surface dissociate, forming new Ti–O bonds at the interface. The stretching vibrations with a shoulder extending from 1045-400 cm^{-1} are related to Ti–O–Ti and Ti–O stretching bands, which are the characteristic peak of TiO_2 [38]. The fingerprint region around 1500 cm-1 ascribed to the inter-atomic vibration is generally associated with the metal oxide absorption band [39]. The increased surface area of the TiO_2 nanoparticles due to the annealing temperature reduces the surface available for water adsorption. According to Figure 9(d), the intensity of the OH absorption band is found to decrease with increased temperatures. The sharpening of the metal oxide's characteristic peaks shows that the crystalline nature of TiO_2 increases with an increase in annealing temperature.

3.8. Photocatalytic analysis

An evaluation of the samples' photocatalytic activity at various temperatures was carried out by the degradation of methylene blue (MB) under artificial UV light. Figure 10(a) shows the MB degradation process using TiO_2 photocatalyst annealed at constant temperature and UV radiated at different times. According to the results, it was observed that the concentration of MB decreased with prolonged UV light exposure

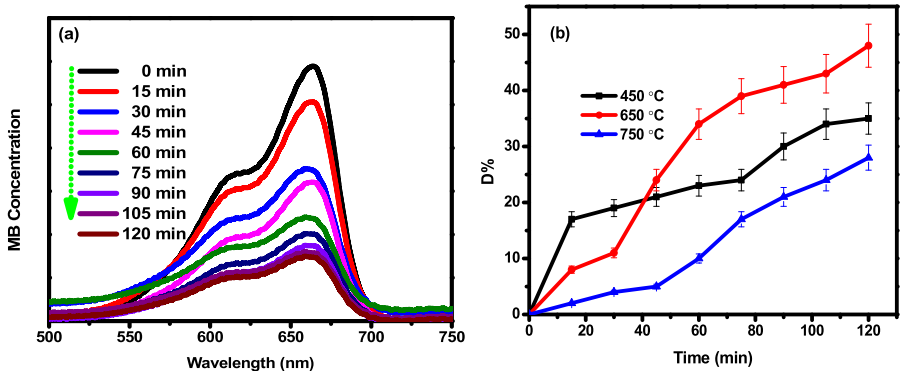

Figure 10. (a) Effect of TiO_2 photocatalyst on the degradation of MB dye under UV light radiations, (b) percent degradation of MB by samples annealed at various temperatures as a function of irradiation time.

time. This was due to the change in the delivery of oxidation radicals from the irradiated NPs, continuously reducing the concentration of oxidizable MB molecules [40]. The degradation of MB can be understood from the beer-lamberts law, where the absorbance obtained from UV is taken to be directly proportional to the MB concentration. The MB efficiency was shown in Figure 10(b), whereby the anatase-rutile mixed-phase had the highest degradation %. However, the photodegradation of MB was assumed to follow the Langmuir-Hinshelwood kinetic model, and its first-order kinetics were expressed according to [41] Equ. (17)

$$InC_A / C_t = kt \tag{17}$$

where C_A is the initial concentration, C_t is the degraded MB concentration at time t (min), and k is the photocatalytic reaction rate.

According to Figure 11(a), the photodegradation rate constants obtained from the slope of the drawn straight line are 0.01266, 0.02434, and 0.01061 for 450 °C, 650 °C, and 750 °C respectively. It shows that the mixed phase's photo-activity was much higher than that of the single anatase and rutile phase. However, the activation energy of the dye was estimated by Equ. (18) [42].

$$\log k = -E_{act}/2.303RT \tag{18}$$

where k is the rate constant, E_{act} the activation energy, R is the constant (8.31 $j/mol^{-1}k^{-1}$) of the gas, while T (300K) is the temperature at which the reaction continued. The E_{act} of 450 °C, 650 °C, and 750 °C were 10,899.89, 9269.20 and 11,340.57 J/mol, respectively. Sample annealed at 650 °C has the highest efficiency, which requires the minimum energy

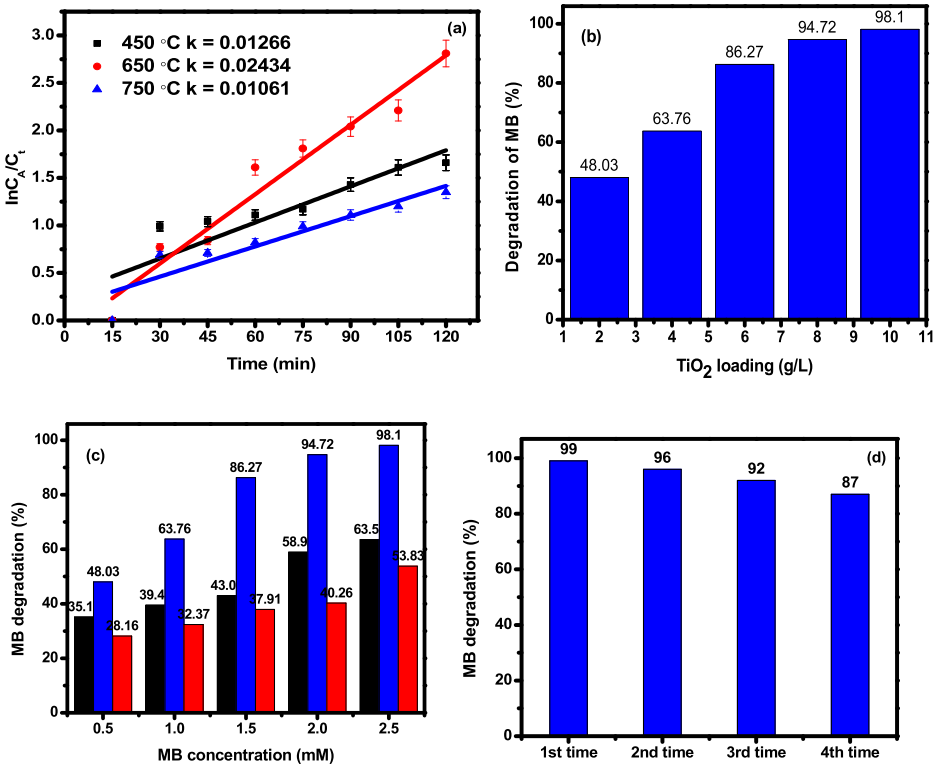

Figure 11. (a) degradation rates for MB with 450 °C (anatase), 650 °C (anatase/rutile mixture) and 750 °C (rutile) as photocatalysts, (b) Effect of TiO_2 loading (sample annealed at 650 °C) on MB at room temperature, (c) Effect of MB concentration on photocatalytic activity of TiO_2 samples under UV light for 120 min, (d) The recyclability of the TiO_2 carried out for four-cycles on the sample annealed at 650 °C.

of activation. The sample at 750 °C has the lowest efficiency hence requires the highest activation energy [42]. The effect of different TiO_2 (mixed-phase) loading on the photoactivity has been investigated, as shown in Figure 11(b). The outcomes show that increasing the amount of TiO_2 improves photocatalytic activity. These findings are based on the fact that higher TiO_2 concentrations provide more reaction sites for water molecule oxidation and hydroxyl radicals formation, resulting in a higher reaction rate [7]. The tests show that the 10 g/L of TiO_2 loading needed further examination. The increase of the surface adsorption site causes a reduction in the time difference during the degradation. Therefore, to facilitate the total breakdown of MB dye, an increase of TiO_2 concentration can completely break down various initial quantities of MB. When the amount of TiO_2 concentration is increased, the time for degradation decreases since the surface adsorption sites are increased. The photocatalytic efficiency of the samples is known to be influenced by the concentration of MB. Thus, TiO_2 photocatalyst has a higher absorbance of the light at low MB concentration. As a result, the photocatalytic activity of TiO_2 annealed at 450 °C, 650 °C, and 750 °C were investigated in this study using different concentrations of MB over a 120-minute irradiation period as shown in Figure 11(c). As the MB concentration increased, more adsorption sites on the solid surface become visible, inhabiting the catalyst particles, and raising the amount of desorbed MB when radiated with the light. An increase in TiO_2 concentration causes a more significant increase in absorbance of light at low MB concentration. The recyclability of 650-TiO_2 was tested for up to four cycles. Figure 11. (d) shows that the prepared nanoparticles are very recyclable. The slight decrease in the photocatalytic activity during each cycle is due to a slight aggregation of the NPs during the photocatalytic process. Therefore, the photocatalyst can be separated and recycled, making it a promising material for environmental remediation.

4. Conclusion

The calcination temperature is found to have a transformative effect on the TiO_2 NPs. The metastable anatase phase is found to transform entirely to rutile at a temperature around 750 °C. EDS data verified the elemental composition of TiO2 NPs and that calcination in the air creates oxygen vacancies. The particle sizes and the agglomeration increased with an increase in calcination temperature. The band-gaps of the TiO_2 NPs reduced from 3.21 to 3.05 eV with the rise in calcination temperature from 450 to 750, ℃ respectively. The PL intensities decreased with an increase in annealing temperatures due to the effect of phase transformation. The methylene blue degradation with the increase in irradiation time was highest in the mixed-phase (anatase/rutile) than in single phases, while anatase was higher than the rutile phase. Therefore, annealing temperature improves the nanomaterial crystallinity, causes phase transformation, and affects photocatalytic activity. Our study suggests that the mixed-phase obtained at 650 °C is the best photocatalyst for water purification due to its performance in the degradation of methylene blue dye.

Declarations

Author contribution statement

Dorah Kawira Muthee: Conceived and designed the experiments; Performed the experiments; Analyzed and interpreted the data; Wrote the paper.

Birhanu Francis Dejene: Conceived and designed the experiments; Analyzed and interpreted the data; Contributed reagents, materials, analysis tools or data.

Funding statement

This work was supported by the National Research Fund, NRF S.A.

Data availability statement

Data will be made available on request.

Declaration of interests statement

The authors declare no conflict of interest.

Additional information

No additional information is available for this paper.

References

[1] D. S. Bagheri Ramimoghadam, S.B.A. Hamid, Biotemplated synthesis of anatase titanium dioxide nanoparticles via lignocellulosic waste material, J. Biomed. Biotechnol. 205636 (2014) 1–8.
[2] X. Yan, Y. Li, T. Xia, Black titanium dioxide nanomaterials in photocatalysis, Int. J. Photoenergy 8529851 (2017) 1–17.
[3] B.K. Mutuma, G.N. Shao, W.D. Kima, H.T. Kim, Sol-gel synthesis of mesoporous anatase–brookite and anatase–brookite–rutile TiO_2 nanoparticles and their photocatalytic properties, J. Colloid Interface Sci. 442 (2015) 1–7.
[4] A.O. Araoyinbo, M.M.A.B. Abdullah, M.A.A.M. Salleh, N.N.A. Aziz, A.I. Azmi, Phase study of titanium dioxide nanoparticlese prepared via sol-gel process, Mater. Sci. Eng. 343 (2018) 12011–12021.
[5] D.K. Muthee, B.F. Dejene, The effect of tetra isopropyl orthotitanate (TIP) concentration on structural and luminescence properties of titanium dioxide nanoparticles prepared by sol-gel method, Mater. Sci. Semicond. Process. 106 (2020) 104783–104791.
[6] A.D. Paola, M. Bellardita, L. Palmisano, Brookite, the least known TiO_2 photocatalyst, Catalysts 3 (2013) 36–73.
[7] C. Xu, G.P. Rangaiah, X.S. Zhao, Photocatalytic degradation of methylene blue by titanium dioxide: experimental and modeling study 53, American Chemical Society, 2014, pp. 14641–14649.
[8] T. Kalaivani, P. Anilkumar, Role of temperature on the phase modification of TiO_2 nanoparticles synthesized by the precipitation method, Silicon 10 (2017) 1679–1686.
[9] M. Chen, Ce Hu, X. Luo, A. Hong, T. Yu, C. Yuan, Ferromagnetic behaviors in monolayer MOS_2 introduced by nitrogen-doping, Appl. Phys. Lett. 116 (2020), 073102.
[10] J. Banjuraizah, Y.P. Ong, Z.A. Ahmad, Effect of calcination temperature on titanium dioxide synthesized by sol-gel method, Int. J. Curr. Sci. Eng. Technol. 1 (2018) 68–74.
[11] A. Ahmad, J. Thiel, S.I. Shah, Structural effects of niobium and silver doping on titanium dioxide nanoparticles, J. Phys. 61 (2007) 11–15.
[12] A.S. Bakri, M.Z. Sahdan, F. Adriyanto, N.A. Raship, N.D.M. Said, S.A. Abdullah, M.S. Rahim, Effect of annealing temperature of titanium dioxide thin films on structural and electrical properties, Am. Inst. Phys. 30030 (2017) 1788–1798.
[13] M. Kumar Singh, M. Singh Mehata, Phase-dependent optical and photocatalytic performance of synthesized titanium dioxide (TiO_2) nanoparticles, Optik - Int. J. Light Electr. Opt. 163011 (2019) 193–204.
[14] N. Yuangpho, D.T.T. Trinh, D. Channei, W. Khanitchaidecha, A. Nakaruk, The influence of experimental conditions on photocatalytic degradation of methylene blue using titanium dioxide particle, J. Austr. Ceram. Soc. 54 (2018) 557–564.
[15] F.B. Dejene, A.G. Ali, H.C. Swart, R.J. Botha, K. Roro, L. Coetsee, Optical properties of ZnO nanoparticles synthesized by varying the sodium hydroxide to zinc acetate molar ratios using a Sol-Gel process, Cent. Eur. J. Phys. 9 (2011) 1321–1326.
[16] M.K. Hossain, M.F. Pervez, M.N.H. Mia, S. Tayyaba, M.J. Uddin, R. Ahamed, Annealing temperature effect on structural, morphological and optical parameters of mesoporous TiO_2 film photoanode for dye-sensitized solar cell application, Mater. Sci. 35 (2017) 868–877.
[17] V.H. Castrejón-Sánchez, R. López, M. Ramón-González, Á. Enríquez-Pérez, M. Camacho-López, G. Villa-Sánchez, Annealing Control on the Anatase/rutile Ratio of Nanostructured Titanium Dioxide Obtained by Sol-Gel. Crystals, 2018.
[18] A.K.M. Muaz, U. Hashim, M.K.M. Arshad, A.R. Ruslinda, R. Ayub, S.C.B. Gopinath, Effect of Annealing Temperature on Structural, Morphological and Electrical Properties of Nanoparticles TiO_2 Thin Films by Sol-Gel Method. Presented at the International Conference on Nano-Electronic Technology Devices and Materials, 2015.
[19] S.T. Hayle, G.G. Gonfa, Synthesis and characterization of titanium oxide nanomaterials using sol-gel method, Am. J. Nanosci. Nanotechnol. 2 (2014) 1–7.
[20] A.M. Luís, M.C. Neves, M.H. Mendon, O.C. Monteiro, Influence of calcination parameters on the TiO_2 photocatalytic properties, Mater. Chem. Phys. 125 (2011) 20–25.
[21] M. Dalvandi, B. Ghasemi, Synthesis of titanium dioxide nanopowder via sol-gel method at ambient temperature, Sol-Gel Sci. Technol. (2013).
[22] K. Thangavelu, R. Annamalai, D. Arulnandhi, Synthesis and characterization of nanosized TiO_2 powder derived from a sol-gel process in acidic conditions, Int. J. Eng. Sci. Emerg. Technol. 4 (2013) 90–95.
[23] S. Mahshid, M. Askari, M.S. Ghamsarib, Synthesis of TiO_2 nanoparticles by hydrolysis and peptization of titanium isopropoxide solution, J. Mater. Process. Technol. 189 (2007) 296–300.

[24] B. Akbari, M.P. Tavandashti, M. Zandrahimi, Particle size characterization of nanoparticles – a practical approach, Iran. J. Mater. Sci. Eng. 8 (2011) 1–9.
[25] F. Amano, E. Ishinaga, A. Yamakata, Effect of particle size on the photocatalytic activity of WO_3 particles for water oxidation, J. Phys. Chem. C 117 (2013) 22584–22590.
[26] A.W. Myint, T.T. Moe, W.Y. Linn, A. Chang, P.P. Win, The effect of heat treatment on phase transformation and morphology of nano-crystalline titanium dioxide (TiO_2), Int. J. Sci. Technol. Res. 6 (2017) 1–7.
[27] P.K. Singh, S. Mukherjee, C.K. Ghosh, S. Maitra, Influence of precursor type on structural, morphological, dielectric and magnetic properties of TiO_2 nanoparticles, J. Cerâm. 63 (2017) 549–556.
[28] A. Sarkar, G.G. Khan, The formation and detection techniques of oxygen vacancies in titanium oxide-based nanostructures, Nanoscale 11 (2019) 3414–3445.
[29] M. Tsega, F.B. Dejene, Structural and optical properties of Ce-Doped TiO_2 nanoparticles using the sol-gel process, ECS J. Solid State Sci. Technol. 5 (2015) 17–20.
[30] S.V. Motloung, F.B. Dejene, O.M. Ntwaeaborwa, H.C. Swart, Effects of catalyst/zinc mole fraction on $ZnAl_2O_4$:0.01% Cr^{3+} nanocrystals synthesized using sol-gel process, Mater. Res. Express 45029 (2014) 3–15.
[31] B. Anitha, M.A. Khadar, Anatase-rutile phase transformation, and photocatalysis in peroxide gel route prepared TiO_2 nanocrystals: role of defect states, Solid State Sci. 108 (2020) 106392–106404.
[32] L.V. Maneeshya, I.J. Berlin, P.V. Thomas, V.S. Anitha, P.B. Nair, K. Joy, Influence of annealing temperature and oxygen atmosphere on the optical and photoluminescence properties of $BaTiO_3$ amorphous thin films prepared by sol-gel method, J. Mater. Sci. Mater. Electron. 24 (2013) 848–854.
[33] L. Castaneda, The particulars properties of annealing temperature and spacer thickness on cross-relaxation and decay dynamics in aluminum oxide upon thulium (III) oxide nanolaminate silicon-based electroluminescent and optoelectronics devices, Opt. Mater. 101 (2020) 109720–109728.
[34] M. Syahin, F.A. Zamri, N. Sapawe, Effect of pH on phenol degradation using green synthesized titanium dioxide nanoparticles, Mater. Today: Proc. 19 (2019) 1321–1326.
[35] G. Tian, K. Pan, H. Fu, L. Jing, W. Zhou, Enhanced photocatalytic activity of Sn-doped TiO_2–ZrO_2 nanoparticles under visible-light irradiation, J. Hazard Mater. 166 (2009) 939–944.
[36] S.M. Hassan, A.I. Ahmed, M.A. Manna, Preparation and characterization of SnO_2 doped TiO_2 nanoparticles: effect of phase changes on the photocatalytic and catalytic activity, J. Sci.: Adv. Mater. Dev. 4 (2019) 400–412.
[37] T. Kalaivani, P. Anilkumar, Role of temperature on the phase modification of TiO_2 nanoparticles synthesized by the precipitation method, Silicon 10 (2018) 1679–1686.
[38] M. Boehme, W. Ensinger, Mixed phase anatase/rutile titanium dioxide nanotubes for enhanced photocatalytic degradation of methylene blue, Nano-Micro Lett. 4 (2011) 236–241.
[39] M.A. Ahmed, E.E. El-Katori, Z.H. Gharni, Photocatalytic degradation of methylene blue dye using Fe_2O_3/TiO_2 nanoparticles prepared by sol-gel method, J. Alloys Compd. 553 (2013) 19–29.
[40] C.B. Hiragond, A.S. Kshirsaga, D.P. Khanna, P.V. More, P.K. Khanna, Electro-photocatalytic degradation of methylene blue dye using various nanoparticles: a demonstration for undergraduates, J. Nanomed. Res. 7 (2018) 254–257.
[41] K. Fujihara, S. Izumi, T. Ohno, M. Matsumura, Time-resolved photoluminescence of particulate TiO_2 photocatalysts suspended in aqueous solutions, J. Photochem. Photobiol. Chem. 132 (2000) 99–104.
[42] H. Park, T. Goto, S. Cho, S. Lee, M. Kakihana, T. Sekino, Effects of annealing temperature on the crystal structure, morphology, and optical properties of peroxo-titanate nanotubes prepared by peroxo-titanium complex ion, Nanomaterials 10 (2020) 1331–1348.